Multi-Sensor Joint Detection and Tracking with the Bernoulli Filter

Ba Tuong Vo, Chong Meng See, Ning Ma and Wee Teck Ng

Abstract

This paper proposes a filter for joint detection and tracking of a single target using measurements from multiple sensors under the presence of detection uncertainty and clutter. To capture the target presence/absence in the surveillance region as well as its kinematic state, we represent the target state as a set that can take on either the empty set or a singleton. The uncertainty in such a set is modeled by a Bernoulli random finite set (RFS), and Bayes optimal estimators for joint detection and tracking are presented. A closed form solution for the linear-Gaussian model is derived and an analytic implementation is proposed for non-linear models based on the unscented transform. We apply the technique to tracking targets constrained to move on roads with TDOA/FDOA measurements.

Index Terms

Random sets, Finite Set Statistics, Bernoulli, Filtering, Multi-Sensor Tracking, Joint Detection and Tracking, TDOA/FDOA Tracking, PHD filter, CPHD filter.

B.-T. Vo is with the school of Electrical Electronic and Computer Engineering, University of Western Australia, Crawley, WA 6009, Australia, Tel: (61) 8 6488 1767, Fax: (61) 8 6488 1065, (email: ba-tuong.vo@uwa.edu.au).

C.-M. See is with DSO National Laboratories, 20 Science Park Drive Singapore 118230 (email: SamsonSee@ntu.edu.sg), Tel: (65) 6592 7750, Fax: (65) 6775 9011

N. Ma is with DSO National Laboratories, 20 Science Park Drive 118230 Singapore, Tel: (65) 6308 1636, Fax: (65) 6775 9011 (email: mning@dso.org.sg).

W.-T. Ng is with DSO National Laboratories, 20 Science Park Drive Singapore 118230 Singapore, Tel: (65) 6776 2255, Fax: (65) 6775 9011 (email: WTNg@ntu.edu.sg).

This research was supported under Australian Research Council's Discovery Projects DP0989007. Dr Ba Tuong Vo is the recipient of an Australian Research Council Post Doctoral Fellowship.

I. Introduction

In surveillance applications, the target of interest may not always be present in the surveillance region. A target can enter and exit the surveillance region at random instances. Moreover, due to background clutter, exact knowledge of target existence in the surveillance area cannot be assumed. A filter that does not account for existence of targets may follow spurious measurements when the target is not in the scene, and when the target enters the scene the tracker may not be able to lock-on to the target. Thus, it is crucial that the filter detects the presence of the target as well as tracking it.

This paper considers the problem of joint detection and tracking of a single target using measurements from multiple sensors under the presence of detection uncertainty and clutter. The use of multiple sensors can, in principle, reduce uncertainty about the target existence as well as its states. However, in the presence of clutter, multiple sensors also introduce ghost targets for certain measurement types such as direction of arrival (DOA), time difference of arrival (TDOA), frequency difference of arrival (FDOA) etc. The ghost target problem becomes increasingly worse with each additional sensor. Traditional solutions have mostly been based on multiple hypothesis tracking (MHT) techniques, for theoretical foundations see [2], [3], [10] and the references therein, while for applications and developments see for example the references [7], [8], [11] amongst the many in the literature.

Using Finite Set Statistics (FISST), we propose a novel and Bayes optimal solution, to the multi-sensor (single-target) joint detection and tracking problem in the presence of detection uncertainty and clutter, which in turn solves the ghost target problem. FISST is a set of tools developed from random finite set (RFS) or point process theory for filtering/estimation problems involving finite sets [16], [18]. This approach has lead to advances in multi-target tracking methodology, notably the Probability Hypothesis Density (PHD) filters [16], [17], which attracted substantial interest in recent years. Particle implementations [34] [29], [39], and Gaussian mixture implementations [35], [36] of the PHD filters have inspired a host of applications and extensions e.g. [31], [4], [12], [14], [23], [24], [25], [33]. Novel and physically intuitive interpretations have also been proposed in [9]. In the single-target realm, RFS or FISST-based single-target multi-sensor tracking has been shown to be Bayes optimal under a very general setting, as well as exhibiting favorable performance [37]. The technique proposed in this paper generalizes that of [37] to perform joint detection and tracking.

To capture the target presence/absence in the surveillance region as well as its kinematic state, we represent the target state as a set that can take on either the empty set or a singleton. The uncertainty in such a set is modelled by a Bernoulli random finite set (RFS). Detection uncertainty and clutter in the

measurements are modelled by the superposition of Bernoulli RFSs and Poisson RFSs as described in [37]. Using RFS models, the joint detection and tracking problem can be posed as a Bayes optimal filtering problem with finite-set-valued states and observations. A closed form solution for the linear-Gaussian model is presented along with an extension to non linear models via the unscented transform. We apply the technique to tracking targets constrained to move on roads with TDOA/FDOA measurements from multiple platforms.

The Bernoulli filter has been suggested for joint detection and tracking in [38] and is similar to the JoTT filter proposed in [18] (see Section 14.7). This work is the first to present a more complete study with implementations and applications. Note also that the Bernoulli filter reduces to the IPDA filter [19] under uniform sensor field of view, uniform clutter, and the merging the Gaussian mixture posterior density into a single Gaussian component assumptions. The Bernoulli filter is consequently more general, optimally handles state-dependent sensor field of view and non uniform clutter, and is derived from a principled top-down approach. The linear Gaussian implementation also coincides with single target MHT when gating of measurements and pruning/merging of hypotheses is performed.

The paper is organized as follows. In Section II, we state notations and summarize the pertinent background material for this paper. This section briefly reviews the classical notions of optimal filtering and Bayes optimality, followed by the basics of RFS theory, and finally RFS based single target tracking or filtering (with multiple sensors) in the presence of detection uncertainty and false alarms, complete with a statement of its Bayes optimality. Section III presents the main contribution of this paper, which builds on the background material in Section II, and generalizes the work in [37], to develop a novel joint detection and tracking filter, and finally to establish its Bayes optimality. Section IV then presents a closed-form solution to this filter under standard linear Gaussian assumptions. Section V subsequently describes a Gaussian mixture implementation applicable to non-linear non-Gaussian models, which is applied, in VI, to a problem where TDOA/FDOA measurements are received by a moving platform consisting of pairs of physical receivers, and where targets are constrained to moving on a network of roads.

II. Background

This section outlines the elements of Bayesian optimal (single) target tracking with multiple sensors that can accommodate clutter (or false alarms), and state dependent sensor field of view (or probability of detection). We first review the simpler problem of tracking with perfect detection and no false measurements in subsection II-A and then move on to the more realistic problem of optimal Bayes

tracking in the presence of detection uncertainty and clutter in subsections II-B and II-C

A. Classical Optimal Filtering

In many dynamic state estimation problems, the state is assumed to follow a Markov process on the state space $\mathcal{X} \subseteq \mathbb{R}^{n_x}$, with *transition density* $f_{k|k-1}(\cdot|\cdot)$, i.e. given a state x_{k-1} at time $k-1$, the probability density of a transition to the state x_k at time k is

$$f_{k|k-1}(x_k|x_{k-1}). \tag{1}$$

For notational simplicity, random variables and their realizations are not distinguished. The Markov process described by the transition (1) is partially observed in the observation space $\mathcal{Z} \subseteq \mathbb{R}^{n_z}$, via a sensor, as modelled by the *likelihood function* $g_k(\cdot|\cdot)$, i.e. given a state x_k at time k, the probability density of receiving the observation $z_k \in \mathcal{Z}$ is

$$g_k(z_k|x_k). \tag{2}$$

In tracking or filtering we are interested in the probability density of the state x_k at time k given all observations $z_{1:k} = (z_1, \ldots, z_k)$ up to time k, denoted by

$$p_k(x_k|z_{1:k}), \tag{3}$$

This conditional probability density, at time k, is the so-called *posterior density* (or *filtering density*). From an initial density $p_0(\cdot)$, the posterior density at time k can be computed using the Bayes recursion

$$p_{k|k-1}(x_k|z_{1:k-1}) = \int f_{k|k-1}(x_k|x)p_{k-1}(x|z_{1:k-1})dx, \tag{4}$$

$$p_k(x_k|z_{1:k}) = \frac{g_k(z_k|x_k)p_{k|k-1}(x_k|z_{1:k-1})}{\int g_k(z_k|x)p_{k|k-1}(x|z_{1:k-1})dx}. \tag{5}$$

Using multiple sensors can reduce uncertainty about the state and hence improve the state estimate. This can be seen from Figure 1 which illustrates an application with direction of arrival (DOA) measurements. With one sensor (see Figure 1.a), the uncertainty is spread along the DOA. However, with two sensors (Figure 1.b) the uncertainty is reduced by the intersection of the DOAs.

[Fig. 1 about here.]

Suppose that there are S mutually independent sensors, i.e. the product of the individual likelihoods for each sensor is the joint likelihood for all sensors. Let $z_k^{(1)}, z_k^{(2)}, ..., z_k^{(S)}$ denote measurements, with individual likelihoods $g_k^{(1)}(z_k^{(1)}|x_k)$, $g_k^{(2)}(z_k^{(2)}|x_k), ..., g_k^{(S)}(z_k^{(S)}|x_k)$, from sensors 1 to S respectively,

and define the augmented measurement $z_k \triangleq (z_k^{(1)}, z_k^{(2)}, ..., z_k^{(S)})$. Since the sensors are independent conditional on x_k, the combined likelihood accounting for all sensor measurements is

$$g_k(z_k|x_k) = \prod_{s=1}^{S} g_k^{(s)}(z_k^{(s)}|x_k).$$

Using the Bayes update (5) with the above likelihood function, the multiple sensor update becomes

$$p_k(x_k|z_{1:k}) = \frac{\prod_{s=1}^{S} g_k^{(s)}(z_k^{(s)}|x_k) p_{k|k-1}(x_k|z_{1:k-1})}{\int \prod_{s=1}^{S} g_k^{(s)}(z_k^{(s)}|x) p_{k|k-1}(x|z_{1:k-1}) dx}. \tag{6}$$

Bayes optimality: A Bayes optimal estimator at time k is any mapping $\hat{x} : z_{1:k} \mapsto \hat{x}(z_{1:k})$ that minimizes the Bayes risk [27],

$$R(\hat{x}) = \mathbb{E}\left[C(x, \hat{x}(z_{1:k}))\right] \tag{7}$$

where $C(x, \hat{x}(z_{1:k}))$ is the penalty assigned to an estimate $\hat{x}(z_{1:k})$ when the true state is x, and $\mathbb{E}$ is the expectation, taken with respect to $p_k(x_k, z_{1:k})$, the joint distribution of the current state x_k and the measurement history $z_{1:k}$. The Bayes risk $R(\hat{x})$ of an estimator $\hat{x}$ can be thought of as the expected penalty for incorrect estimation over all realizations of the state and measurement history. It is well-known in estimation theory that the conditional mean (with respect to the posterior density) is a Bayes optimal estimator corresponding to the penalty $C(x, y) = \|x - y\|^2$.

It can be shown from the Bayes recursion (4)-(5), that

$$R(\hat{x}) = \int \int \int C(x_k, \hat{x}(z_{1:k})) g_k(z_k|x_k) p_{k|k-1}(x_k|z_{1:k-1}) P_{1:k-1}(dz_{1:k-1}) dx_k dz_k.$$

where $P_{1:k-1}$ denotes the distribution of the measurement history up to time $k-1$. The presence of the probability density $g_k(z_k|x_k)$, indicates that the notion of Bayes risk and subsequently, optimality, rest on a well-defined notion of probability density and integration on the measurement space.

B. Detection Uncertainty and Clutter

In practice, the sensor may not detect the measurement generated by the target. In addition, the sensor receives a set of spurious false measurements. At each sampling instant, the sensor effectively receives an unordered finite set of measurements $Z_k \subset \mathcal{Z}$, and it is not known which of these measurements (if any) is from the target [1], [2], [18].

Since the observations are finite sets, the concept of a random finite set is necessary to cast the tracking problem in the Bayesian framework. In essence, a *random finite set* (RFS) is simply a finite-set-valued random variable. An RFS can be specified by a discrete probability distribution that describes the cardinality (number of points) of the set and a family of joint distributions that describes the distribution

of the values of the points. Detailed treatments of RFSs in the context of target tracking can be found in [18], [38]. In the following we outline some elementary tools for RFSs.

1) Belief Density: Let X be an RFS on $\mathcal{X} \subseteq \mathbb{R}^n$, with cardinality denoted by $|X|$, then X is a random variable taking values in, $\mathcal{F}(\mathcal{X})$, the space of finite subsets of $\mathcal{X}$. Since, the space $\mathcal{F}(\mathcal{X})$ does not inherit the usual Euclidean notion of integration and density, the Bayes update (5) is not directly applicable. To develop the notion of integration and probability density for RFSs, we need to invoke measure theoretic arguments. Fortunately Mahler's FISST provides a suitable notion of integration and density that can be applied to our problems without recourse to measure theory.

FISST provides an alternative notion of probability for an RFS X via the *belief functional* β, defined by

$$\beta(S) = \mathbb{P}(X \subseteq S) \tag{8}$$

for all closed $S \subseteq \mathcal{X}$, where $\mathbb{P}(\mathcal{E})$ denotes probability of the event $\mathcal{E}$ [18]. For the modelling of multi-target systems, the belief functional is more convenient than the probability distribution, since the former deals with closed subsets of $\mathcal{X}$ whereas the latter deals with subsets of $\mathcal{F}(\mathcal{X})$. The belief functional can be considered as the RFS analogue to the concept of a cumulative distribution function for vector valued random variables. Using the FISST notion of integration and density, the belief density π of an RFS satisfies for any closed $S \subseteq \mathcal{X}$

$$\beta(S) = \int_{X \subseteq S} \pi(X) \delta X$$

where the set integral is defined by

$$\int_{X \subseteq S} \pi(X) \delta X = \sum_{i=0}^{\infty} \frac{1}{i!} \int_{S^i} \pi(\{x_1, ..., x_i\}) dx_1 \cdots dx_i. \tag{9}$$

with S^i denoting the ith Cartesian product of S. The belief density can similarly be considered as the RFS analogue to the concept of the density function for vector valued random variables. The FISST belief density π of an RFS can also be obtained by taking the FISST set derivative of the belief functional β (see [18] for details). It turns out that the FISST density π is equivalent to the measure theoretic probability density [34]. Subsequently, in this work we do not distinguish between the FISST belief density and the probability density.

2) PHD: The *intensity function* of an RFS X on $\mathcal{X}$, also known in tracking as the *Probability Hypothesis Density* (PHD), is a non-negative function v on $\mathcal{X}$ such that for each region $S \subseteq \mathcal{X}$ [6], [30]

$$\mathbb{E}\left[|X \cap S|\right] = \int_S v(x) dx, \tag{10}$$

where $|X|$ denotes the cardinality (number of elements) of X. In other words, the integral of v over any region S gives the expected number of elements of X that are in S. The local maxima of the PHD v are points in $\mathcal{X}$ with the highest local concentration of expected number of elements, and can be used to generate estimates for the elements of X. The PHD or intensity function is the first-order statistical moment of an RFS, analogous to the concept of an expectation for vector valued random variables.

3) Poisson RFS: An RFS X on $\mathcal{X}$ is said to be *Poisson* with a given *intensity function* v (defined on $\mathcal{X}$) if its cardinality is Poisson distributed with mean $\langle v, 1\rangle$, and for any given cardinality, the elements x of X are independently and identically distributed (i.i.d.) according to the probability density $v(\cdot)/\langle v, 1\rangle$ [6], [30], where $\langle v, h\rangle = \int v(x)h(x)dx$ is the standard notation for the inner product. A Poisson RFS is completely characterized by its intensity function, also known in the tracking literature as the *Probability Hypothesis Density* (PHD).The probability density of a Poisson RFS can also be explicitly expressed in terms of v:

$$\pi(X) = e^{-\langle v,1\rangle} v^X,$$

where

$$v^X = \prod_{x \in X} v(x).$$

Poisson RFSs are useful in modelling births of new targets as well as false measurements or clutter.

4) Bernoulli RFS: A *Bernoulli* RFS on $\mathcal{X}$ has probability $1 - r$ of being empty, and probability r of being a singleton whose (only) element is distributed according to a probability density p (defined on $\mathcal{X}$). The cardinality distribution of a Bernoulli RFS is a Bernoulli distribution with parameter r. The probability density of a Bernoulli RFS is

$$\pi(X) = \begin{cases} 1 - r & X = \emptyset, \\ r \cdot p(x) & X = \{x\}, \\ 0 & otherwise. \end{cases} \tag{11}$$

Bernoulli RFSs are useful in modelling detection uncertainty.

C. Filtering in Detection Uncertainty and Clutter

Suppose at time k that the target is in state x_k. The measurement process is given by the RFS measurement equation

$$Z_k = \Theta_k(x_k) \cup K_k, \tag{12}$$

where $\Theta_k(x_k)$ is the RFS of the target-generated measurement, and K_k is the RFS of clutter. It is assumed that conditional on x_k, $\Theta_k(x_k)$, and K_k are independent RFSs. The spurious set of measurements or

clutter is modelled as a Poisson RFS with intensity κ_k, while the target generated measurement $\Theta_k(x_k)$ is modelled as a Bernoulli RFS with parameters $\{p_{D,k}(x_k), g_k(\cdot|x_k)\}$, where $p_{D,k}(x_k)$ is the probability of detection, and $g_k(z|x_k)$ is the likelihood of the target generated measurement z.

The probability density of the measurement Z_k is given by [18], [37].

$$\eta_k(Z_k|x) = \frac{(1-p_{D,k}(x))\,\kappa_k^{Z_k} + p_{D,k}(x)\sum\limits_{z\in Z_k} g_k(z|x)\kappa_k^{Z_k-\{z\}}}{e^{\langle \kappa_k, 1\rangle}} \tag{13}$$

As a function of Z_k, the likelihood (13) is a true probability density (up to a scaling constant that cancels the unit of measurement) on $\mathcal{F}(\mathcal{Z})$ in a measure theoretic context [37]. Subsequently, Bayes rule applies and the update equation is

$$p_k(x_k|Z_{1:k}) = \frac{\eta_k(Z_k|x_k)p_{k|k-1}(x_k|Z_{1:k-1})}{\langle \eta_k(Z_k|\cdot), p_{k|k-1}(\cdot|Z_{1:k-1})\rangle}. \tag{14}$$

In the presence of detection uncertainty and clutter, the advantage of using multiple sensors is no longer obvious as illustrated by Figure 2. Contrary to the clutter-free case (see Figure 1.b) in which the target can be located by the intersection of the DOAs, the intersection of cluttered DOAs from the two sensors results in many ghost targets.

[Fig. 2 about here.]

Let $Z_k^{(1)}, Z_k^{(2)}, ..., Z_k^{(S)}$ denote measurements with individual likelihoods $\eta_k^{(1)}(Z_k^{(1)}|x_k)$, $\eta_k^{(2)}(Z_k^{(2)}|x_k)$, ... , $\eta_k^{(S)}(Z_k^{(S)}|x_k)$, from sensors 1 to S, respectively, and define the augmented measurement $Z_k \triangleq (Z_k^{(1)}, Z_k^{(2)}, ..., Z_k^{(S)})$. Since the sensors are independent conditional on x_k, the combined likelihood accounting for all sensor measurements is

$$\eta_k(Z_k|x_k) = \prod_{s=1}^{S} \eta_k^{(s)}(Z_k^{(s)}|x_k). \tag{15}$$

and the multiple sensor update can be written as

$$p_k(x_k|Z_{1:k}) = \frac{\prod_{s=1}^{S} g_k^{(s)}(Z_k^{(s)}|x_k)p_{k|k-1}(x_k|Z_{1:k-1})}{\left\langle \prod_{s=1}^{S} \eta_k^{(s)}(Z_k^{(s)}|\cdot), p_{k|k-1}(\cdot|Z_{1:k-1})\right\rangle}. \tag{16}$$

To gain an intuition for how the multi-sensor Bayes filter (4)-(16) addresses the ghost target problem, consider the multi-sensor DOA measurements depicted in Figure 2. Assuming a uniform prior, after the measurement update from the 1st sensor, the probability masses representing uncertainty in the target are spread out along the DOAs. After the update from the 2nd sensor, the uncertainty in the target contracts into modes near the intersections of the DOAs. Since the prior is uniform, the modes of the posterior

will have similar heights, and it is not possible to distinguish which mode corresponds to the target. The prediction then propagates the modes of the posterior forward in accordance with the target dynamics. At the next time step, the product of the likelihoods, i.e. the joint likelihood, also has several modes due to clutter. However, only the mode that corresponds to the target is corroborated by the prediction. The modes that correspond to (the intersection of) clutter returns do not follow the dynamical model and hence are not supported by the prediction. The event that the intersections of the clutter DOAs following the target dynamic is extremely rare. Consequently, after the update step, which multiplies the prediction density with the joint likelihood, the mode that corresponds to the target will have a high weight because it is reinforced by the prediction, whereas the modes that correspond to clutter will diminish. Hence, after several time steps, the mode that corresponds to the target emerges and the modes that correspond to clutter die out.

Bayes optimality: Since the measurement likelihoods (13) and (15) are probability densities in the finite-set-valued measurement, using the FISST set integral, the Bayes risk is given by

$$R(\hat{x}) = \mathbb{E}\left[C(x, \hat{x}(Z_{1:k}))\right] \tag{17}$$

$$= \int\int\int C(x, \hat{x}(Z_{1:k}))g_k(Z_k|x)p_{k|k-1}(x|Z_{1:k-1})P_{1:k-1}(dZ_{1:k-1})dx\delta Z_k. \tag{18}$$

This is a mathematically well-defined quantity. Hence, it follows that the conditional mean (with respect to the posterior probability density) computed via the single-sensor or multi-sensor update (16) is Bayes optimal.

Bayes optimality of traditional methods for tracking in clutter such as multiple hypothesis tracking (MHT) and probabilistic data association (PDA) have not been established. Moreover, their complexity does not scale gracefully with the number of sensors. Multi-sensor MHT is generally computationally intensive and the multi-sensor PDA (MSPDA) filter is more popular. While MSPDA is less expensive than MHT, it is still computationally demanding because this approach requires filtering with an augmented measurement set formed by the Cartesian product of measurement sets from all sensors [20].

III. Joint Detection and Estimation

In a number of practical applications, especially passive sensing, we cannot assume that the target to be tracked is always in the scene. A target can enter and exit the surveillance region at random instances. A tracker that does not account for existence of targets may follow spurious measurements when the target is not in the scene, and when the real target enters the scene the tracker may not be able to lock-on to the target. In addition, missed detections may also be encountered as a result of disturbances, sensor

imperfections, and even non communicative targets. It is, therefore, important to consider techniques that can jointly detect and track a target.

In this section, we propose the Bernoulli filter–an extension of the RFS single-target Bayes recursion to the more general problem of single-target joint detection and estimation. The Bernoulli filter is presented in subsection III-A, followed by Bayes optimal estimators for joint detection and tracking in subsection III-B.

A. The Bernoulli Filter

In a joint detection estimation problem, it is assumed that at most one target can be present, and that the target can be in one of two 'present' or 'absent' modes. Thus, we model the target state X_k, at time k, as a Bernoulli RFS with probability density given by

$$\pi_k(X_k) = \begin{cases} 1 - r_k, & X_k = \emptyset \\ r_k p_k(x_k), & X_k = \{x_k\} \\ 0, & \text{otherwise} \end{cases}$$

where r_k is the probability of target existence and p_k is the density of the kinematic state of the target.

For the dynamical model, suppose that the state X_{k-1} at time $k-1$ is a Bernoulli RFS. Conditional upon $X_{k-1} = \emptyset$, the target can re-enter the scene with probability $p_{R,k}$ and occupy kinematic state x_k with probability density $f_{R,k}(x_k)$, or remain absent from the scene with probability $1 - p_{R,k}$. More concisely, X_k is the Bernoulli RFS described by

$$f_{k|k-1}(X_k|\emptyset) = \begin{cases} 1 - p_{R,k}, & X_k = \emptyset, \\ p_{R,k} f_{R,k}(x_k), & X_k = \{x_k\} \\ 0, & \text{otherwise} \end{cases} .$$

In addition, conditional upon $X_{k-1} = \{x_{k-1}\}$, with probability $p_{S,k}(x_{k-1})$ the target can survive to the next time step and transition to x_k with probability density $f_k(x_k|x_{k-1})$, or disappear with probability $1 - p_{S,k}(x_{k-1})$. In other words X_k is the Bernoulli RFS described by

$$f_{k|k-1}(X_k|\{x_{k-1}\}) = \begin{cases} 1 - p_{S,k}(x_{k-1}), & X_k = \emptyset, \\ p_{S,k}(x_{k-1}) f_{k|k-1}(x_k|x_{k-1}) & X_k = \{x_k\} \\ 0, & \text{otherwise} \end{cases} .$$

For the measurement model, suppose that the state X_k at time k is a Bernoulli RFS. Conditional upon $X_k = \{x_k\}$, the measurements follow the model previously stated in (12) and the likelihood of receiving the measurement Z_k from state x_k is $\eta_k(Z_k|x_k)$ defined in (13). Moreover, conditional upon $X_k = \emptyset$, all

measurements must originate from clutter and Z_k reduces to K_k and the likelihood is $e^{-\langle 1,\kappa_k\rangle}\kappa_k^{Z_k}$ where $\kappa_k(\cdot)$ is the intensity of the clutter RFS K_k. Hence, the likelihood of the measurement set Z_k at time k is

$$\gamma_k(Z_k|X_k) = \begin{cases} e^{-\langle 1,\kappa_k\rangle}\kappa_k^{Z_k}, & X_k = \emptyset \\ \eta_k(Z_k|x_k), & X_k = \{x_k\} \\ 0, & \text{otherwise} \end{cases}.$$

Under these assumptions, an exact recursion for the posterior density can easily be obtained as stated in the following proposition.

Proposition 1: If the posterior density π_{k-1} at time $k-1$ is a Bernoulli given by $\pi_{k-1} = \{r_{k-1}, p_{k-1}\}$, then the predicted density $\pi_{k|k-1}$ to time k is also a Bernoulli and is given by $\pi_{k|k-1} = \{r_{k|k-1}, p_{k|k-1}\}$ where

$$r_{k|k-1}=p_{R,k}(1 - r_{k-1}) + r_{k-1} \langle p_{S,k}, p_{k-1}\rangle , \tag{19}$$

$$p_{k|k-1}(x_k)=\frac{p_{R,k}(1 - r_{k-1})}{r_{k|k-1}} f_{R,k}(x_k) + \frac{r_{k-1}}{r_{k|k-1}} \left\langle f_{k|k-1}(x_k|\cdot), p_{S,k}(\cdot)p_{k-1}(\cdot)\right\rangle . \tag{20}$$

Moreover, the updated density π_k at time k is also a Bernoulli and is given by $\pi_k = \{r_k, p_k\}$ where

$$r_k=\frac{\left\langle \eta_k(Z_k|\cdot), p_{k|k-1}(\cdot)\right\rangle}{\frac{(1-r_{k|k-1})}{r_{k|k-1}} e^{-\langle 1,\kappa_k\rangle}\kappa_k^{Z_k} + \left\langle \eta_k(Z_k|\cdot), p_{k|k-1}(\cdot)\right\rangle}, \tag{21}$$

$$p_k(x_k)=\frac{\eta_k(Z_k|x_k)p_{k|k-1}(x_k)}{\left\langle \eta_k(Z_k|\cdot), p_{k|k-1}(\cdot)\right\rangle}. \tag{22}$$

Proof: The prediction is obtained by substituting the relevant expressions in Mahler's multi-target Bayes prediction:

$$\begin{aligned} \pi_{k|k-1}(X)=&\int f_{k|k-1}(X|X_{k-1})\pi_{k-1}(X_{k-1})\delta X_{k-1} \\ =&f_{k|k-1}(X|\emptyset)\pi_{k-1}(\emptyset) + \int f_{k|k-1}(X|\{\zeta\})\pi_{k-1}(\{\zeta\})d\zeta \\ =&\begin{cases} (1-p_{R,k})(1-r_{k-1}) + r_{k-1}\int(1-p_{S,k}(\zeta))p_{k-1}(\zeta)d\zeta, & X = \emptyset \\ p_{R,k}(1-r_{k-1})f_{R,k}(x) + r_{k-1}\int f_{k|k-1}(x|\zeta)p_{S,k}(\zeta)p_{k-1}(\zeta)d\zeta, & X = \{x\} \\ 0, & \text{otherwise} \end{cases}. \end{aligned}$$

Note that $\pi_{k|k-1}(\emptyset) + \int\pi_{k|k-1}(\{x\})dx = 1$, hence $\pi_{k|k-1}$ is a Bernoulli density with parameters $r_{k|k-1} = \int\pi_{k|k-1}(\{x\})dx$ and $p_{k|k-1}(x) = \pi_{k|k-1}(\{x\})/\int\pi_{k|k-1}(\{x\})dx$ as stated.

The update is obtained by substituting the relevant expressions in Mahler's multi-target Bayes update

$$\pi_k(X_k) = \frac{\gamma_k(Z_k|X_k)\pi_{k|k-1}(X)}{\int\gamma_k(Z_k|X)\pi_{k|k-1}(X)\delta X}.$$

Consequently,

$$\gamma_k(Z_k|X_k)\pi_{k|k-1}(X_k) = \begin{cases} (1-r_{k|k-1})e^{-\langle 1,\kappa_k\rangle}\kappa_k^{Z_k}, & X_k = \emptyset \\ \eta_k(Z_k|x)r_{k|k-1}p_{k|k-1}(x), & X_k = \{x\} \\ 0, & \text{otherwise} \end{cases}$$

and

$$\int \gamma_k(Z_k|X)\pi_{k|k-1}(X)\delta X = (1-r_{k|k-1})e^{-\langle 1,\kappa_k\rangle}\kappa_k^{Z_k} + r_{k|k-1}\int \eta_k(Z_k|x)p_{k|k-1}(x)dx.$$

Note that $\pi_k(\emptyset) + \int \pi_k(\{x\})dx = 1$, hence π_k is a Bernoulli density with parameters $r_k = \int \pi_{k|k-1}(\{x\})dx$ and $p_k(x) = \pi_k(\{x\})/\int \pi_k(\{x\})dx$ as stated. ■

Notice that the propagation of the probability of target existence r_k is now coupled to the propagation of the distribution p_k of the kinematic state.

For multiple sensors, we can apply the Bernoulli update iteratively as follows: Use the measurement and parameters of sensor 1 to calculate $\{r_k^{(1)}, p_k^{(1)}\}$ via (21), (22); use $p_k^{(1)}$ as the prior, and use the measurement and parameters of sensor 2 to calculate$\{r_k^{(2)}, p_k^{(2)}\}$ via (21), (22), and so on until we exhaust the list of sensors. More concisely, let $\eta_k^{(s)}(Z_k^{(s)}|x)$ denote the likelihood of the measurement set $Z_k^{(s)}$ collected by the sth sensor at time k, given the kinematic state x, and define an update operator $\Psi_k^{(s)}$ on any Bernoulli $\{r, p\}$ by

$$\left[\Psi_k^{(s)} r\right] = \frac{\left\langle \eta_k^{(s)}(Z_k^{(s)}|\cdot), p(\cdot)\right\rangle}{\frac{(1-r)}{r}e^{-\left\langle 1,\kappa_k^{(s)}\right\rangle} + \left\langle \eta_k^{(s)}(Z_k^{(s)}|\cdot), p(\cdot)\right\rangle}$$

$$\left[\Psi_k^{(s)} p\right](x) = \frac{\eta_k^{(s)}(Z_k^{(s)}|x)p(x)}{\left\langle \eta_k^{(s)}(Z_k^{(s)}|\cdot), p(\cdot)\right\rangle}$$

where the parameters of the sth sensor are denoted by the superscript (s), e.g. $\kappa_k^{(s)}(\cdot), p_{D,k}^{(s)}(\cdot), g_k^{(s)}(\cdot|\cdot)$. Then, the multi-sensor updated Bernoulli parameters are:

$$r_k = \Psi_k^{(S)} \circ \cdots \circ \Psi_k^{(2)} \circ \Psi_k^{(1)} r_{k|k-1}$$

$$p_k = \Psi_k^{(S)} \circ \cdots \circ \Psi_k^{(2)} \circ \Psi_k^{(1)} p_{k|k-1}$$

where $\circ$ denotes a composition.

B. Bayes Optimal Estimator for Joint Detection and Tracking

In the following, let X_k denote the state at time k, $\pi_k(\cdot|Z_{1:k})$ denote its posterior density, $\rho_k(\cdot|Z_{1:k})$ denote its posterior cardinality distribution (a Bernoulli distribution with parameter r_k).

1) Marginal Multi-Object Estimator: The Marginal Multi-Object (MaM) estimator is defined as a two-step estimator. First, the cardinality is estimated using a MAP estimate on the posterior cardinality distribution (the posterior distribution of the number of targets $|X|$)

$$\hat{n} = \arg\sup_{n} \rho_k(n|Z_{1:k}). \tag{23}$$

Second, the states are estimated using a MAP estimate on the posterior density given that $n = \hat{n}$ (the posterior density restricted to $|X| = \hat{n}$)

$$\hat{X}^{MaM} = \arg \sup_{X:|X|=\hat{n}} \pi_k(X|Z_{1:k}). \tag{24}$$

It has been shown that the MaM estimator is Bayes optimal, however convergence results are not currently known [18].

2) Joint Multi-Object Estimator: The Joint Multi-Object (JoM) estimator for Bernoulli posterior is defined as

$$\hat{X}_c^{JoM} = \arg\sup_{X} \pi_k(X|Z_{1:k}) \frac{c^{|X|}}{|X|!}. \tag{25}$$

where c is a dimensionless constant. It has been shown that the JoM estimator is Bayes optimal, and is statistically consistent [18], with respect to the Matheron topology and subsequently the Optimal SubPattern Assignment metric [28]. Additionally, the value of c determines the desired accuracy for the state estimate and the rate of convergence of the estimator (smaller c provides better accuracy with slower convergence, and vice-versa).

IV. Closed Form Solution and Gaussian Mixture Implementation

In general, the Bayes recursion does not admit an analytic solution. However, a closed form solution to this recursion can be derived under linear Gaussian assumptions. Additionally, the problem can be solved using sequential Monte Carlo techniques. In this section, a closed form solution to the RFS single-target Bayes recursion (4, 14) is derived for the special class of linear Gaussian single-target models. Hereon, for notational compactness we drop the dependence on the measurement history in the posterior and predicted densities, i.e.

$$p_k(x_k) \triangleq p_k(x_k|Z_{1:k})$$

$$p_{k|k-1}(x_k) \triangleq p_{k|k-1}(x_k|Z_{1:k-1})$$

A. Prediction and Update for Linear Gaussian Model

In addition to linear Gaussian transition and likelihood

$$f_{k|k-1}(x|\zeta) = \mathcal{N}(x; F_{k-1}\zeta, Q_{k-1}), \tag{26}$$

$$g_k(z|x) = \mathcal{N}(z; H_k x, R_k), \tag{27}$$

$$f_{R,k}(x) = \sum_{i=1}^{J_{R,k}} w_{R,k}^{(i)} \mathcal{N}(x; x_{R,k}^{(i)}, Q_{R,k}^{(i)}) \tag{28}$$

the linear Gaussian single-target model assumes a constant sensor field of view, i.e.

$$p_{S,k}(x) = p_{S,k}$$

$$p_{D,k}(x) = p_{D,k}.$$

The following propositions establish an exact closed form solution to the recursion (4),(14) for the linear Gaussian single-target model.

Proposition 2: Under linear Gaussian assumptions, if the posterior density π_{k-1} at time $k-1$ is a Bernoulli given by $\pi_{k-1} = \{r_{k-1}, p_{k-1}\}$, with p_{k-1} being a Gaussian mixture of the form

$$p_{k-1}(x) = \sum_{j=1}^{J_{k-1}} w_{k-1}^{(j)} \mathcal{N}(x; m_{k-1}^{(j)}, P_{k-1}^{(j)}), \tag{29}$$

then,

$$r_{k|k-1} = p_{R,k}(1 - r_{k-1}) + r_{k-1} p_{S,k}, \tag{30}$$

$$p_{k|k-1}(x) = \frac{p_{R,k}(1-r_{k-1})}{r_{k|k-1}} \sum_{i=1}^{J_{R,k}} w_{R,k}^{(i)} \mathcal{N}(x; x_{R,k}^{(i)}, Q_{R,k}^{(i)}) + \frac{r_{k-1} p_{S,k}}{r_{k|k-1}} \sum_{i=1}^{J_{k-1}} w_{k-1}^{(i)} \mathcal{N}(x; m_{k|k-1}^{(i)}, P_{k|k-1}^{(i)}), \tag{31}$$

where

$$m_{k|k-1}^{(i)} = F_{k-1} m_{k-1}^{(i)}, \tag{32}$$

$$P_{k|k-1}^{(i)} = Q_{k-1} + F_{k-1} P_{k-1}^{(i)} F_{k-1}^{T}. \tag{33}$$

Proposition 3: Under linear Gaussian assumptions, if the predicted density $\pi_{k|k-1}$ is a Bernoulli given by $\pi_{k|k-1} = \{r_{k|k-1}, p_{k|k-1}\}$, with $p_{k|k-1}$ being a Gaussian mixture of the form

$$p_{k|k-1}(x) = \sum_{j=1}^{J_{k|k-1}} w_{k|k-1}^{(j)} \mathcal{N}(x; m_{k|k-1}^{(j)}, P_{k|k-1}^{(j)}), \tag{34}$$

then,

$$r_k = \frac{(1-p_{D,k})\kappa_k^{Z_k} + p_{D,k}\sum\limits_{z\in Z_k}\sum\limits_{j=1}^{J_{k|k-1}}\kappa_k^{Z_k-\{z\}}w_{k|k-1}^{(j)}q_k^{(j)}(z)}{\frac{(1-r_{k|k-1})}{r_{k|k-1}}\kappa_k^{Z_k} + (1-p_{D,k})\kappa_k^{Z_k} + p_{D,k}\sum\limits_{z\in Z_k}\sum\limits_{j=1}^{J_{k|k-1}}\kappa_k^{Z_k-\{z\}}w_{k|k-1}^{(j)}q_k^{(j)}(z)} \tag{35}$$

$$p_k(x) = \frac{(1-p_{D,k})\kappa_k^{Z_k}p_{k|k-1}(x) + p_{D,k}\sum\limits_{z\in Z_k}\sum\limits_{j=1}^{J_{k|k-1}}\kappa_k^{Z_k-\{z\}}w_{k|k-1}^{(j)}q_k^{(j)}(z)\mathcal{N}(x;m_{k|k}^{(j)}(z),P_{k|k}^{(j)}),}{(1-p_{D,k})\kappa_k^{Z_k} + p_{D,k}\sum\limits_{z\in Z_k}\sum\limits_{j=1}^{J_{k|k-1}}\kappa_k^{Z_k-\{z\}}w_{k|k-1}^{(j)}q_k^{(j)}(z)} \tag{36}$$

where

$$q_k^{(j)}(z) = \mathcal{N}(z;\eta_{k|k-1}^{(j)},S_{k|k-1}^{(j)}), \tag{37}$$

$$\eta_{k|k-1}^{(j)} = H_k m_{k|k-1}^{(j)}, \tag{38}$$

$$S_{k|k-1}^{(j)} = H_k P_{k|k-1}^{(j)} H_k^T + R_k, \tag{39}$$

$$m_{k|k}^{(j)}(z) = m_{k|k-1}^{(j)} + K_k^{(j)}(z-\eta_{k|k-1}^{(j)}), \tag{40}$$

$$P_{k|k}^{(j)} = P_{k|k-1}^{(j)} - P_{k|k-1}^{(j)}H_k^T[S_{k|k-1}^{(j)}]^{-1}H_k P_{k|k-1}^{(j)} \tag{41}$$

$$K_k^{(j)} = P_{k|k-1}^{(j)}H_k^T[S_{k|k-1}^{(j)}]^{-1}. \tag{42}$$

Proposition 2 provides closed form expressions for computing the existence probability $r_{k|k-1}$ and the means, covariances and weights of $p_{k|k-1}$ from those of p_{k-1} and r_{k-1}. Proposition 3 then provides closed form expressions for computing the updated existence probability r_k and the means, covariances and weights of p_k from those of $p_{k|k-1}$ and $r_{k|k-1}$ when a new measurement arrives. Note also that the recursion from Propositions 2 and 3 simplifies to the Kalman filter when $J_{k-1}=1,\ p_{S,k}=1$, $r_{k-1}=1$, $p_{D,k}=1$, $\kappa_k=0$ and $Z_k=\{z_k\}$.

B. Multiple Sensor Updates for Linear Gaussian Model

For multiple sensors, we can apply Proposition 3 iteratively as follows: Use the measurement and parameters of sensor 1 to calculate $p_k^{(1)}$ via Proposition 2; use $p_k^{(1)}$ as the prior and the measurement and parameters of sensor 2 to calculate $p_k^{(2)}$ via Proposition 2, and so on until we exhaust the list of sensors.

More concisely, denote for each $s = 1, \ldots, S$,

$$\begin{aligned} Z_k^{(s)} &= \text{measurement set from sensor } s \text{ at time } k \\ p_{D,k}^{(s)} &= \text{probability of detection of sensor } s \text{ at time } k, \\ \kappa_k^{(s)} &= \text{clutter intensity of sensor } s \text{ at time } k \\ H_k^{(s)} &= \text{measurement matrix of sensor } s \text{ at time } k, \\ R_k^{(s)} &= \text{noise covariance of sensor } s \text{ at time } k. \end{aligned}$$

Then the update operator $\Psi_k^{(s)}$ on any Bernoulli $\{r, p\}$ with

$$p = \sum_{j=1}^{J} w^{(j)} \mathcal{N}(\cdot; m^{(j)}, P^{(j)})$$

becomes

$$\left[\Psi_k^{(s)} r\right] = \frac{(1 - p_{D,k}^{(s)})(\kappa_k^{(s)})^{Z_k^{(s)}} + p_{D,k}^{(s)} \sum\limits_{z \in Z_k^{(s)}} \sum\limits_{j=1}^{J} (\kappa_k^{(s)})^{Z_k^{(s)} - \{z\}} w^{(j)} q_k^{(s,j)}(z)}{\frac{(1-r)}{r} e^{-\langle 1, \kappa_k^{(s)} \rangle} + (1 - p_{D,k}^{(s)})(\kappa_k^{(s)})^{Z_k^{(s)}} + p_{D,k}^{(s)} \sum\limits_{z \in Z_k^{(s)}} \sum\limits_{j=1}^{J} (\kappa_k^{(s)})^{Z_k^{(s)} - \{z\}} w^{(j)} q_k^{(s,j)}(z)}$$

$$\left[\Psi_k^{(s)} p\right](x) = \frac{(1 - p_{D,k}^{(s)})(\kappa_k^{(s)})^{Z_k^{(s)}} p(x) + p_{D,k}^{(s)} \sum\limits_{z \in Z_k^{(s)}} \sum\limits_{j=1}^{J} (\kappa_k^{(s)})^{Z_k^{(s)} - \{z\}} w^{(j)} q_k^{(s,j)}(z) \mathcal{N}(x; m_k^{(s,j)}(z), P_k^{(s,j)}),}{(1 - p_{D,k}^{(s)})(\kappa_k^{(s)})^{Z_k^{(s)}} + p_{D,k}^{(s)} \sum\limits_{z \in Z_k^{(s)}} \sum\limits_{j=1}^{J} (\kappa_k^{(s)})^{Z_k^{(s)} - \{z\}} w^{(j)} q_k^{(s,j)}(z)}$$

where

$$q_k^{(s,j)}(z) = \mathcal{N}(z; \eta_k^{(s,j)}, S_k^{(s,j)}), \tag{43}$$

$$\eta_k^{(s,j)} = H_k^{(s)} m^{(,j)}, \tag{44}$$

$$S_k^{(s,j)} = H_k^{(s)} P^{(j)} H_k^{(s)T} + R_k^{(s)}, \tag{45}$$

$$m_k^{(s,j)}(z) = m_k^{(j)} + K_k^{(s,j)}(z - \eta_k^{(s,j)}), \tag{46}$$

$$P_k^{(s,j)} = P^{(j)} - P^{(j)} H_k^{(s)T} [S_k^{(s,j)}]^{-1} H_k^{(s)} P^{(j)} \tag{47}$$

$$K_k^{(s,j)} = P^{(j)} H_k^{(s)T} [S_k^{(s,j)}]^{-1}. \tag{48}$$

C. Pruning, Merging and Capping of Gaussians

The number of Gaussian components required to exactly represent the posterior density increases without bound. In implemementations then, to limit the growth of the number of components with time,

a standard pruning and merging procedure can be used. This procedure is summarized as follows. If at time k the posterior density p_k is given and is of the form

$$p_k(x) = \sum_{j=1}^{J_k} w_k^{(j)} \mathcal{N}(x; m_k^{(j)}, P_k^{(j)}),$$

it is approximated by a pruned and merged version

$$\hat{p}_k(x) \approx \sum_{j=1}^{J_{\max}} \hat{w}_k^{(j)} \mathcal{N}(x; \hat{m}_k^{(j)}, \hat{P}_k^{(j)}),$$

in which components with weights $w_k^{(j)}$ below a threshold T' are discarded, components with means $m_k^{(j)}$ within a distance U' of each other are merged, and only the $J_{\max}$ components with the highest weights are retained. Specifically, begin by identifying components with weights below a threshold T' and pruning/discarding all others:

$$I_k = \{i = 1, ..., J_k : w_k^{(i)} > T'\}.$$

Next, from the remaining components, identify the component with the highest weight and group together all components within a weighted distance U' of the highest peak:

$$\begin{aligned} j &= \arg\max_{i \in I_k} w_k^{(i)}, \\ L_k &= \{i \in I_k : (m_k^{(i)} - m_k^{(j)})^T (P_k^{(i)})^{-1} (m_k^{(i)} - m_k^{(j)}) < U'\}. \end{aligned}$$

Merge the group by replacing it with a single Gaussian given by the weighted average of those in the group:

$$\begin{aligned} \hat{w}_k^{(\ell)} &= \sum_{i \in L_k} w_k^{(i)}, \\ \hat{m}_k^{(\ell)} &= \frac{1}{\hat{w}_k^{(\ell)}} \sum_{i \in L_k} w_k^{(i)} m_k^{(i)}, \\ \hat{P}_k^{(\ell)} &= \frac{1}{\hat{w}_k^{(\ell)}} \sum_{i \in L_k} w_k^{(i)} (P_k^{(i)} + (\hat{m}_k^{(\ell)} - m_k^{(i)})(\hat{m}_k^{(\ell)} - m_k^{(i)})^T). \end{aligned}$$

Then, excluding components that have already been merged, repeat the grouping and merging process until all components have been accounted for. Finally, select the $J_{\max}$ merged components with the highest weights, and set $\{\hat{w}_k^{(\ell)}, \hat{m}_k^{(\ell)}, \hat{P}_k^{(\ell)}\}$ as the pruned and merged approximation to the posterior density.

V. Non-Linear Extension

This section describes an implementation of the Bernoulli filter for nonlinear models using the unscented transform. Subsection V-A describes the relevant nonlinear dynamic and measurement model while subsection V-B describes how the unscented transform is used to approximate the prediction and update step of the Bernoulli filter. Subsection V-C details how state dependent sensor field of view can be incorporated into this implementation. Subsection V-D shows how dynamical constraints such as road map information can be exploited to improve performance.

A. Dynamic and Measurement Models

The unscented Gaussian mixture approximation for tracking a single target proposed in [37] is an efficient and reliable technique that can address the non-linearity in tracking with road constraints and non-linear measurements. This approach is applicable to state and measurement transformations of the form:

$$x_k = f_k(x_{k-1}, w_{k-1}),$$
$$z_k = h_k(x_k, v_k),$$

where f_k and h_k are the non-linear transition and measurement functions respectively, and w_{k-1} and v_k are independent zero-mean Gaussian noise processes with covariance matrices Q_{k-1} and R_k respectively (i.e. these replace the original linear Gaussian assumptions in (26) and (27) respectively). The model considered in this paper is a special case of the above model with additive Gaussian noise:

$$f_k(x_{k-1}, w_k) = \psi_k(x_{k-1}) + Gw_{k-1},$$
$$h_k(x_k, v_k) = \varphi_k(x_k) + v_k.$$

B. Unscented Approximation

Analogous to the UKF, the unscented Gaussian mixture approximation recursion applies the unscented transform to analytically propagate means and covariances through the (non-linear) transition and measurement functions φ_k and h_k respectively as follows. Given a Gaussian mixture posterior density, at time $k-1$,

$$p_{k-1}(x) = \sum_{j=1}^{J_{k-1}} w_{k-1}^{(j)} \mathcal{N}(x; m_{k-1}^{(j)}, P_{k-1}^{(j)}),$$

for each mixture component $j = 1, ..., J_{k-1}$ of the posterior density p_{k-1} , use the unscented transform with mean $\mu_k^{(j)}$ and covariance $C_k^{(j)}$ given by

$$\mu_k^{(j)} = \begin{bmatrix} m_{k-1}^{(j)} & 0^T & 0^T \end{bmatrix}^T,$$
$$C_k^{(j)} = \text{diag}(P_{k-1}^{(j)}, Q_{k-1}, R_k),$$

to generate a set of sigma points $\{y_k^{(j,\ell)}\}_{\ell=0}^{L}$ and weights $\{u_k^{(j,\ell)}\}_{\ell=0}^{L}$. Then, partition the sigma points into

$$y_k^{(j,\ell)} = [(x_{k-1}^{(j,\ell)})^T, (w_{k-1}^{(j,\ell)})^T, (v_k^{(j,\ell)})^T]^T$$

for $\ell = 0, \ldots, L$ and proceed as follows.

1) Unscented Gaussian Mixture Prediction: In the unscented Gaussian mixture prediction, the previous mixture components are predicted forward via the unscented transform by

- propagating the sigma points through the transition function according to $x_{k|k-1}^{(j,\ell)} = f_k(x_{k-1}^{(j,\ell)}, w_{k-1}^{(j,\ell)})$ for $\ell = 0, \ldots, L$ and
- replacing the original expressions (32)-(33) with the approximations (49)-(50).

As a result, the expressions for the predicted probability of existence and density are the same as those given in Proposition 2, but with

$$m_{k|k-1}^{(j)} = \sum_{\ell=0}^{L} u_k^{(j,\ell)} x_{k|k-1}^{(j,\ell)}, \tag{49}$$
$$P_{k|k-1}^{(j)} = \sum_{\ell=0}^{L} u_k^{(j,\ell)} (x_{k|k-1}^{(j,\ell)} - m_{k|k-1}^{(j)})(x_{k|k-1}^{(j,\ell)} - m_{k|k-1}^{(j)})^T. \tag{50}$$

2) Unscented Gaussian Mixture Update: In the unscented Gaussian mixture update, the predicted mixture components are measurement-corrected via the unscented transform. This is achieved by

- propagating the sigma points through the measurement function according to $z_{k|k-1}^{(j,\ell)} = h_k(x_{k|k-1}^{(j,\ell)}, v_k^{(j,\ell)})$ for $\ell = 0, \ldots, L$,
- replacing the original equations (38)-(39) with the approximations (52)-(53), and
- replacing the originals equations(41)-(42) with the approximations (55)-(56).

As a result, the expressions for the updated probability of existence and posterior density are the same as those given in Proposition 3, but with

$$q_k^{(j)}(z) = \mathcal{N}(z; \eta_{k|k-1}^{(j)}, S_{k|k-1}^{(j)}), \tag{51}$$

$$\eta_{k|k-1}^{(j)} = \sum_{\ell=0}^{L} u_k^{(j,\ell)} z_{k|k-1}^{(j,\ell)}, \tag{52}$$

$$S_{k|k-1}^{(j)} = \sum_{\ell=0}^{L} u_k^{(j,\ell)} (z_{k|k-1}^{(j,\ell)} - \eta_{k|k-1}^{(j)})(z_{k|k-1}^{(j,\ell)} - \eta_{k|k-1}^{(j)})^T, \tag{53}$$

$$m_{k|k}^{(j)}(z) = m_{k|k-1}^{(j)} + m_{k|k-1}^{(j)} + K_k^{(j)}(z - \eta_{k|k-1}^{(j)}), \tag{54}$$

$$P_{k|k}^{(j)} = P_{k|k-1}^{(j)} - G_k^{(j)}[S_k^{(j)}]^{-1}[G_k^{(j)}]^T, \tag{55}$$

$$K_k^{(j)} = G_k^{(j)}[S_{k|k-1}^{(j)}]^{-1}, \tag{56}$$

$$G_k^{(j)} = \sum_{\ell=0}^{L} u_k^{(j,\ell)} (x_{k|k-1}^{(j,\ell)} - m_{k|k-1}^{(j)})(z_{k|k-1}^{(j,\ell)} - m_{k|k-1}^{(j)})^T. \tag{57}$$

For multiple sensors, we can apply the unscented Gaussian mixture update above iteratively similar to the procedure described in subsection IV-B.

C. Non-Uniform Sensor Field of View

The Bayes update (14) accommodates state dependent probability of detection $p_D(x)$. However, the unscented Gaussian mixture update assumes a constant probability of detection. While this update can be extended to handle state dependent probability of detection (see [37]), the computational requirement increases. More importantly, the updated posterior density becomes a Gaussian mixture with positive and negative weights, which makes the reduction of components in the Gaussian mixture more complex. In this work we adopt the simple approach used in [33] to handle state dependent probability of detection.

Consider Bayes update equation (14), which involves $[1 - p_{D,k}(x)]\, p_{k|k-1}(x)$ and $p_{D,k}(x)p_{k|k-1}(x)g_k(z|x)$ where the predicted density is a Gaussian mixture (34). Following [33], we apply the following approximation

$$[1 - p_{D,k}(x)]\, p_{k|k-1}(x) \approx \sum_{i=1}^{J_{k|k-1}} [1 - P_{D,k}(\ m_{k|k-1}^{(i)})] w_{k|k-1}^{(i)} \mathcal{N}(x; m_{k|k-1}^{(i)}, P_{k|k-1}^{(i)}). \tag{58}$$

Further, noting that, using the unscented Kalman update step outlined in subsection V-B2,

$$g_k(z|x)\mathcal{N}(x; m_{k|k-1}^{(i)}, P_{k|k-1}^{(i)}) \approx q_k^{(i)}(\ z)\mathcal{N}(x; m_{k|k}^{(i)}(z), P_{k|k}^{(i)}) \tag{59}$$

where $q_k^{(i)}(\ z), m_{k|k}^{(i)}(z)$, and $P_{k|k}^{(i)}$ are given by (51), (54) and (55) respectively. Following [33] we apply the following approximation

$$p_{D,k}(x)g_k(z|x)p_{k|k-1}(x) \approx \sum_{i=1}^{J_{k|k-1}} p_{D,k}(\ m_{k|k}^{(i)}(z))w_{k|k-1}^{(i)}q_k^{(i)}(\ z)\mathcal{N}(x; m_{k|k}^{(i)}(z), P_{k|k}^{(i)}). \tag{60}$$

Hence,

$$r_k \approx \frac{\sum_{i=1}^{J_{k|k-1}} \left(\kappa_k^Z[1-p_{D,k}(m_{k|k-1}^{(i)})]w_{k|k-1}^{(i)} + \sum_{z\in Z}\kappa_k^{Z-\{z\}}p_{D,k}(m_{k|k}^{(i)}(z))w_{k|k-1}^{(i)}q_k^{(i)}(z)\right)}{\frac{(1-r_{k|k-1})}{r_{k|k-1}}\kappa_k^Z + \sum_{i=1}^{J_{k|k-1}} \left(\kappa_k^Z[1-p_{D,k}(m_{k|k-1}^{(i)})]w_{k|k-1}^{(i)} + \sum_{z\in Z}\kappa_k^{Z-\{z\}}p_{D,k}(m_{k|k}^{(i)}(z))w_{k|k-1}^{(i)}q_k^{(i)}(z)\right)} \tag{61}$$

$$p_k(x) \approx \frac{\sum_{i=1}^{J_{k|k-1}} \left(\kappa_k^Z[1-p_{D,k}(m_{k|k-1}^{(i)})]w_{k|k-1}^{(i)}\mathcal{N}(x; m_{k|k-1}^{(i)}, P_{k|k-1}^{(i)}) + \sum_{z\in Z}\kappa_k^{Z-\{z\}}p_{D,k}(m_{k|k}^{(i)}(z))w_{k|k-1}^{(i)}q_k^{(i)}(z)\mathcal{N}(x; m_{k|k}^{(i)}(z), P_{k|k}^{(i)})\right)}{\sum_{i=1}^{J_{k|k-1}} \left(\kappa_k^Z[1-p_{D,k}(m_{k|k-1}^{(i)})]w_{k|k-1}^{(i)} + \sum_{z\in Z}\kappa_k^{Z-\{z\}}p_{D,k}(m_{k|k}^{(i)}(z))w_{k|k-1}^{(i)}q_k^{(i)}(z)\right)} \tag{62}$$

D. Road Constraints

The incorporation of prior information such as road map constraints can improve the accuracy of the tracking algorithm. In this subsection we adapt the unscented Gaussian mixture filter described in subsection V to accommodate road map constraints. There exist sophisticated techniques for exploiting road constraints to improve tracking performance, see for example [32], [15], [21], [33]. Techniques such as variable structure IMM can be expensive since we have to deal with a large number of Gaussians. In this work, we use a simple projection approach to illustrate that road map information can be easily incorporated in the Bernoulli filter.

We first present a model to describe the road map constrained target dynamics. This model is then used in conjunction with a constant turn motion model and the unscented transform to perform the nonlinear prediction step that accounts for road map constraints. Experiments are reported to illustrate the difference in performance of the proposed algorithm between scenarios with and without road map information.

1) Road Model: Roads are described by a list of trapezoidal segments, see Figure 3. A segment consists of a tuple of 4 points, for example the ith segment in figure 3 consists of the tuple (P_1, P_2, P_3, P_4). The midpoint M_{12} of the line segment joining P_1, P_2 and the midpoint M_{34} of the line segment joining P_3, P_4 defines a direction t_i on the road which approximates the road direction throughout the segment. Any curved road can be reasonably approximated by a set of trapezoidal segments using this approach.

[Fig. 3 about here.]

2) Motion Model with Road Constraints: The constant turn model (70) allows targets to move over the entire surveillance region and does not constrain the targets to be on the roads. To incorporate road constraints into the target dynamics, we need a transition density that models the constant turn dynamic while having zero (or negligible) mass off the roads. One way of achieving this is to use a transition density $f_{k|k-1}(\cdot|x)$ with negligible mass off the road while approximating the constant turn model (70) in some sense. Noting that the transition density for the constant turn model is a Gaussian with mean $\psi_k(x)$, we model target dynamics with road constraints by a Gaussian with mean being the projection of $\psi_k(x)$ onto the road. The covariance matrix of our Gaussian transition density is chosen to model uncertainty in the tangential and normal directions to the road. This is explained more precisely below.

Suppose that x is the current state. Let $\tilde{x}$ denote the mean $\psi_k(x)$ of the next state conditioned on x, and S_i denotes the road segment closest to $\tilde{x}$ in Euclidean distance, or, if desired in the Mahalanobis distance. Then the projection $\tilde{x}^{\perp}$ of the mean $\tilde{x}$ onto S_i consists of position, velocity and turn-rate components given by

$$\tilde{x}_p^{\perp} = M_i + t_i t_i^T \left(\tilde{x}_p - M_i\right) \tag{63}$$

$$\tilde{x}_v^{\perp} = t_i t_i^T \tilde{x}_v \tag{64}$$

$$\tilde{x}_{\omega}^{\perp} = \tilde{x}_{\omega} \tag{65}$$

where the subscripts p, v and ω are used to indicate the position, velocity and turn-rate components of a state respectively, M_i denotes the midpoint of segment S_i, and t_i denotes the (normalized) tangent direction of segment S_i (see figure 3). The projected vector $\tilde{x}$ is used as the mean of our Gaussian transition density $f_{k|k-1}(\cdot|x)$.

Since the targets are constrained on the road, the covariance matrix $G\text{diag}(\sigma_{\dot{x}}^2, \sigma_{\dot{y}}^2, \sigma_{\omega}^2)G^T$ (see (72)) is no longer adequate for modelling the dynamic noise. The covariance of our Gaussian transition density $f_{k|k-1}(\cdot|x)$ can be chosen by specifying uncertainties in the tangential and normal directions. In the tangential direction, the standard deviations for position and velocity uncertainties are $\sigma_{p^{\parallel}}$ and $\sigma_{v^{\parallel}}$ respectively. Similarly, in the normal direction the standard deviations for position and velocity uncertainties are $\sigma_{p^{\perp}}$, and $\sigma_{v^{\perp}}$. Note that $\sigma_{v^{\perp}}$ is chosen to be much smaller than $\sigma_{v^{\parallel}}$ since we want to constrain the targets to move along the road. The standard deviation for turn-rate uncertainty is σ_{ω}. These model parameters are then converted into the global coordinates to form the covariance matrix,

$\tilde{P}$, in accordance to orientation of the road segment S_i, as follows

$$L_p = \begin{bmatrix} \cos(\phi) & -\sin(\phi) \\ \sin(\phi) & \cos(\phi) \end{bmatrix} \begin{bmatrix} \sigma_{p^{\parallel}} & 0 \\ 0 & \sigma_{p^{\perp}} \end{bmatrix} \tag{66}$$

$$L_v = \begin{bmatrix} \cos(\phi) & -\sin(\phi) \\ \sin(\phi) & \cos(\phi) \end{bmatrix} \begin{bmatrix} \sigma_{v^{\parallel}} & 0 \\ 0 & \sigma_{v^{\perp}} \end{bmatrix} \tag{67}$$

$$L = \begin{bmatrix} L_p(1,1) & 0 & 0 & 0 & 0 \\ 0 & L_v(1,1) & 0 & 0 & 0 \\ L_p(2,1) & 0 & L_p(2,2) & 0 & 0 \\ 0 & L_v(2,1) & 0 & L_v(2,2) & 0 \\ 0 & 0 & 0 & 0 & \sigma_{\omega} \end{bmatrix} \tag{68}$$

$$\tilde{P} = LL^T \tag{69}$$

where $\phi = \arctan(t_{i,y}/t_{i,x})$ denoting the orientation of tangent direction t_i, and $L_x(i,j)$ is the (i,j)-th element of matrix L_x.

3) Prediction with Road Constraints: With the dynamic model proposed above, the unscented Gaussian mixture filter described in the previous subsection can be applied to track multiple targets from non-linear measurements with road constraints. Ideally the posterior density p_{k-1}, and the transition density $f_{k|k-1}(\cdot|x)$ should have zero mass off the road. In this case, the predicted density will also have zero mass of the road. However, as we are approximating p_{k-1}, and $f_{k|k-1}(\cdot|x)$ by functions that has small, but non-zero mass, off the road, the predicted density $p_{k|k-1}$ also has non-zero mass off the road. Moreover, due to the smoothing property of integration, the prediction tends to smear out the probability density and as a result the off-road probability mass can be significant. Our strategy is to apply the unscented Kalman prediction using the constant turn model (70) and then project the resulting density back onto the road so that the off-road mass is reduced.

When using the road model, the predicted mean of the Gaussian components is projected onto the closest road segment. In the vicinity of road crossings, multiple projections to each of the link segments are calculated.

4) Pruning of Off-Road Components: In addition to the Gaussian mixture reduction by pruning and merging, we can further improve performance by using the road constraints to eliminate off-road Gaussian components. This can be simply achieved by removing any components that are further away than a given threshold from the road.

VI. Examples with TDOA/FDOA Measurement

In this section, we apply the proposed technique to jointly detect and track an on road target from TDOA/FDOA measurements received from several moving platforms. We present studies for tracking with and without road map information. Subsections VI-A, VI-B, VI-C, detail the nonlinear dynamic model, the TDOA/FDOA measurement model and scenario settings for this experiment. Subsection VI-D describes the error metric for performance evaluation. Subsections VI-E, VI-F present the experiment results for Bernoulli filtering without and with road map information respectively.

A. Constant Turn Dynamic Model

A generic constant-turn model is adopted. A constant-turn model, as opposed to a constant-velocity model, is expected to enable more accurate tracking on curved roads as well as to better accommodate sharp turns performed by the target. We consequently model the target state at time k by a 5-D vector $x_k = [\ p_{x,k}, \dot{p}_{x,k}, p_{y,k}, \dot{p}_{y,k}, \omega_k]^T$, consisting of the x-coordinate, x-velocity, y-coordinate, y-velocity and turn rate, and whose dynamics is described by the following state transition equation

$$x_k = \psi_k(x_{k-1}) + Gw_{k-1} \tag{70}$$

where

$$\psi_k(x_{k-1}) = \begin{bmatrix} 1 & \frac{\sin(\omega_{k-1}T)}{\omega_{k-1}} & 0 & \frac{\cos(\omega_{k-1}T)-1}{\omega_{k-1}} & 0 \\ 0 & \cos(\omega_{k-1}T) & 0 & -\sin(\omega_{k-1}T) & 0 \\ 0 & \frac{1-\cos(\omega_{k-1}T)}{\omega_{k-1}} & 1 & -\frac{\sin(\omega_{k-1}T)}{\omega_{k-1}} & 0 \\ 0 & \sin(\omega_{k-1}T) & 0 & \cos(\omega_{k-1}T) & 0 \\ 0 & 0 & 0 & 0 & 1 \end{bmatrix} x_{k-1}, \tag{71}$$

$$G = \begin{bmatrix} \frac{T^2}{2} & 0 & 0 \\ T & 0 & 0 \\ 0 & \frac{T^2}{2} & 0 \\ 0 & T & 0 \\ 0 & 0 & T \end{bmatrix}, \tag{72}$$

$T = 1s$ is the sampling period, $w_{k-1} = [w_{\dot{x},k-1}, w_{\dot{x},k-1}, w_{\omega,k-1}]^T$ is a vector of velocities and turn-rate noise components, which are zero-mean Gaussian with standard deviations $\sigma_{\dot{x}} = \sigma_{\dot{y}} = 5m/s$ and $\sigma_\omega = 6^\circ/s$ respectively.

B. TDOA/FDOA Measurement Model

Estimation is performed with TDOA/FDOA measurements. These measurements are calculated from the output of a pair of physical receivers which are specifically deployed to monitor target emissions or reflections. The physical receiver pair can then be treated as a single virtual sensor which gives rise to a TDOA/FDOA measurements. Consequently, as far as the filtering and estimation is concerned, the TDOA/FDOA measurements originate from the so called virtual sensor for which a statistical model can be constructed as follows.

Given a target position $p_k = (p_{x,k,}, p_{y,k,})$ and target velocity $\dot{p}_k = (\dot{p}_{x,k,}, \dot{p}_{y,k,})$, as well as a pair of physical sensors with positions $s_k^{(1)} = (s_{x,k,}^{(1)}, s_{y,k,}^{(1)})$, $s_k^{(2)} = (s_{x,k}^{(2)}, s_{y,k}^{(2)})$ and velocities $\dot{s}_k^{(1)} = (\dot{s}_{x,k,}^{(1)}, \dot{s}_{y,k,}^{(1)})$, $\dot{s}_k^{(2)} = (\dot{s}_{x,k}^{(2)}, \dot{s}_{y,k}^{(2)})$ respectively at time k, and a wave carrier frequency f_c and propagation speed c for the sensor signals, then, the observation model for the (pair) *physical receivers* or (single) *virtual sensor* yielding the FDOA and TDOA pair z_k is given by

$$z_k = (z_{k,T}, z_{k,F}) + v_k \tag{73}$$

where

$$z_{k,T} = \frac{1}{c}\left(\left\|p_k - s_k^{(1)}\right\| - \left\|p_k - s_k^{(2)}\right\|\right),$$
$$z_{k,F} = \frac{f_c}{c}\left(\frac{\left(p_k - s_k^{(1)}\right)\cdot\left(\dot{p}_k - \dot{s}_k^{(1)}\right)}{\left\|p_k - s_k^{(1)}\right\|} - \frac{\left(p_k - s_k^{(2)}\right)\cdot\left(\dot{p}_k - \dot{s}_k^{(2)}\right)}{\left\|p_k - s_k^{(2)}\right\|}\right),$$

v_k is zero mean Gaussian noise with covariance $R_k = \mathrm{diag}([\ \sigma_\tau^2, \sigma_F^2\ ]^T)$, $\sigma_\tau = 10^{-8}s$, $\sigma_F = 1Hz$, and $c = 3 \times 10^8 m/s$ is the propagation speed for EM waves, $\cdot$ denotes the vector dot product.

Each virtual sensor is modeled as having a state or virtual state, comprising its x-coordinate, x-velocity, y-coordinate, y-velocity and turn rate. The virtual state of each physical sensor pair is modelled by the 'midpoint' of the two physical sensor states. The probability of detection for measurements is dependent on the sensor state (or virtual state). A Gaussian sensor model dependent only upon position is adopted as follows. Let $s_k = (s_{x,k}, s_{y,k})$ denote the x and y positions of the sensor state or virtual state at time k. Then, the probability of detection $p_{D,k}(x)$ of a hypothetical target state x and time k is

$$p_{D,k}(x) = \frac{P_{D,\max}}{\mathcal{N}(s_k; s_k, r_{D,k}^2 I_2)}\mathcal{N}([p_{x,k}, p_{y,k}]; s_k, r_{D,k}^2 I_2), \tag{74}$$

where $P_{D,\max}$ is a constant indicating the maximum probability of detection, and $r_{D,k}$ is a constant indicating the standard sensor range, i.e. at s_k the value of at $P_{D,k}(\cdot)$ is $P_{D,\max}$, and a distance $r_{D,k}$ from s_k the value of $P_{D,k}(\cdot)$ drops to approximately 60% of $P_{D,\max}$. Clutter for the virtual sensor follows

a uniform spatial distribution and a Poisson cardinality distribution. Two virtual sensors with the following parameters are considered. For the first virtual sensor, $P_{D,\max} = 0.95$, $r_{D,k} = 4000m$ and the average rate of clutter is $\lambda = 100$ returns per scan. For the second virtual sensor, $P_{D,\max} = 0.75$, $r_{D,k} = 4000m$ and the average rate of clutter is $\lambda = 10$ returns per scan. Clutter for both virtual sensors is uniformly distributed over the region $[-10^{-5}, +10^{-5}]s \times [-200, +200]Hz$.

The combination of the TDOA and FDOA measurements with multiple virtual sensors is expected to yield strong tracking performance, despite the low observability of each measurement type individually, as the information in the measurement can be considered complementary.

C. Scenario Settings

For each example that follows, the following road constraints and target ground truths are used as indicated in Figure 4. Roads are indicated by thin blue lines. The target track is given by a thick red line and a large dot indicating the starting position. The target is born at time $k = 7$ and dies at $k = 93$. This is a 2D example involving 4 roads and 4 intersections, with the target traveling from the top right hand corner downwards along the road and later making a turn at the intersection. Note that all units of time in this section are given in seconds.

For the measurements, two pairs of physical receivers are deployed, where each pair is used to extract a TDOA/FDOA pair. Note again that detection and tracking is performed on the basis of TDOA/FDOA measurement pairs. and that as far as the filtering is concerned, each pair of physical receivers is treated as a single virtual sensor, which is described by a corresponding statistical model. Thus there are two virtual sensors. The physical receiver trajectories and target tracks, are shown in the xy plane in Figure 4.

Mixture component pruning is performed with a threshold of $T' = 10^{-3}$, component merging with a threshold of $U' = 4m$, and a maximum of $J_{\max} = 200$ components is enforced. A target state is declared present by the filter if the estimated existence probability is greater than 0.5, and the actual state estimate is obtained by extracting the mean of the posterior component with the highest weight.

[Fig. 4 about here.]

D. Miss-Distance

We use the Optimal Sub-Pattern Assignment (OSPA) distance between the estimated and true multi-target state as the estimation error since it jointly captures differences in cardinality and individual elements between two finite sets in a mathematically consistent yet intuitively meaningful way [28].

For joint detection and tracking we only need the OSPA distance between two finite sets with cardinality of at most one. The construction of the OSPA distance $d_{OSPA}^{(c)}(X,Y)$ between two finite sets X and Y with cardinality of at most one is as follows. $d_{OSPA}^{(c)}(\emptyset,\emptyset) = 0$, $d_{OSPA}^{(c)}(\{x\},\{y\}) = \min(\|x-y\|, c)$, $d_{OSPA}^{(c)}(\{x\},\emptyset) = d_{OSPA}^{(c)}(\emptyset,\{x\}) = c$ ($500m$ in our example). The OSPA distance is interpreted as a per-target error, comprised of a per-target localization error and a per-target cardinality error. The cut-off parameter c determines the relative weighting of the penalties assigned to cardinality and localization errors. For further details see [28].

E. Bernoulli Filtering without Road Map Information

This section presents the performance of the single target joint detection and tracking filter without road map information. Figures 5 and 6 shows the measurements for each virtual sensor against time.

[Fig. 5 about here.]

[Fig. 6 about here.]

The initial prior consists of a zero probability of existence $r_0 = 0$ and a spatial density $p_0(\cdot)$ which is Gaussian with zero mean $m_0 = [\ 0m, 0ms^{-1}, 0m, 0ms^{-1}, 0rads^{-1}\ ]^T$ and relatively diffuse covariance $R_0 = diag([2000, 2000, 2000, 2000, 0.2]^2)$ (having appropriately squared units). The birth parameters are given by a reentry probability $p_{R,k} = 0.07$ and a reentry density $f_{R,k}(\cdot)$ which is a single Gaussian with an off centre mean $m_{R,k} = [\ 1800m, 0ms^{-1}, 1700m, 0ms^{-1}, 0rads^{-1}\ ]^T$ and relatively diffuse covariance $R_{R,k} = diag([2000, 2000, 2000, 2000, 0.2]^2)$ (having appropriately squared units).

Without road constraints, the filter is completely unable to detect the presence of the target. The OSPA errors are consequently shown to saturate in Figure 7. The poor performance in this case is not a demonstration of the failure of the Bernoulli joint detection and tracking filter. It is actually due to the difficulty of a joint detection and tracking scenario involving TDOA/FDOA measurements, and the relatively high clutter rate for virtual sensor 1 as well as the relatively low detection probability of virtual sensor 2.

[Fig. 7 about here.]

F. Bernoulli Filtering with Road Map Information

This section presents experimental results for the joint detection and tracking filter with road map information. For direct comparison, the previous experiments will be repeated using exactly the same

data, models and parameters except that the filtering is performed with road constraints, i.e. the dynamical model is still based upon the constant turn motion equations, but modified to impose road constraints, and pruning of off-road components is performed after the update step. The parameters for the dynamic model with road constraints is given in the table below.

Parameters	Values
Std. Dev. tangential position $\sigma_{p^{\parallel}}$	$50m/s$
Std. Dev.. normal position $\sigma_{p^{\perp}}$	$10m/s$
Std. Dev. tangential velocity $\sigma_{v^{\parallel}}$	$30m/s$
Std. Dev.. normal velocity $\sigma_{v^{\perp}}$	$15m/s$
Std. Dev. projected turn $\sigma_{\breve{\omega}}$	$6^{\circ}/s$
Threshold for off-road pruning	1.7

The initial prior and birth parameters are also kept the same as before. Figure 8 shows the filter output using only the measurements from the first receiver pair or virtual sensor, while Figure 9 shows the filter output when the measurements from both receiver pairs or virtual sensors are used. The corresponding OSPA errors are shown in Figures 10 and 11. It can be seen that performance is much better than without road information, the true track has been identified and deleted, and when the target is present, it is tracked very accurately. With only one virtual sensor, track confirmation occurs with a $4s$ delay while track termination does not occur before the scenario finishes. With both virtual sensors, the confirmation and termination of the track both occur with $2s$ delays respectively.

[Fig. 8 about here.]

[Fig. 9 about here.]

[Fig. 10 about here.]

[Fig. 11 about here.]

As expected, using measurements from both virtual sensors yields better result than a single virtual sensor. This is verified by Figure 12 which shows the OSPA distance averaged over 100 Monte Carlo runs.

[Fig. 12 about here.]

VII. Conclusions

A Bernoulli filter has been proposed for joint detection and tracking of a single target using measurements from multiple sensors under the presence of detection uncertainty and clutter. Bayes optimal estimators for joint detection and tracking have also been established. A closed form solution to this recursion has been derived under linear Gaussian assumptions. Moreover, an analytic implementation for non-linear non-Gaussian models has been proposed. The technique has been successfully applied to joint detection and tracking problem with road constraints and multiple sensors yielding TDOA/FDOA measurements. The main difficulties encountered were the presence of ghost targets due to the use of multiple sensors, and the inability to initiate tracks due to the high clutter and/or low detection rate of the sensors. Without road map information, estimation performance was poor, however with the incorporation of road map constraints, estimation performance was very good.

References

[1] Bar-Shalom Y. and Fortmann T. E.; *Tracking and Data Association*. San Diego: Academic Press, 1988.

[2] Blackman, S. S. and Popoli R.; *Design and Analysis of Modern Tracking Systems*. Norwood, MA: Artech House, 1999.

[3] Blackman, S. S.; *Multiple-Target Tracking with Radar Applications*. Dedham, MA: Artech House, 1986.

[4] Clark, D.; Ruiz, I.T.; Petillot, Y.; Bell, J.; "Particle PHD filter multiple target tracking in sonar images," *IEEE Transactions on Aerospace and Electronic Systems*, Volume 43, Issue 1, January 2007 Page(s):409 – 416.

[5] Clark, D.E.and Bell, J.; "Multi-target state estimation and track continuity for the particle PHD filter," *IEEE Transactions on Aerospace and Electronic Systems*, Volume 43, Issue 4, October 2007.

[6] Daley, D. and Vere-Jones, D.; *An introduction to the theory of point processes*, Springer-Verlag, 1988.

[7] Daun, M. and Koch, W.; "Multistatic target tracking for non-cooperative illumination by DAB/DVB-T," *Proc. IEEE Radar Conf.*, Rome, Italy, 2008.

[8] Daun, M. and Berger, C.R.; "Track initialization in a multistatic DAB/DVB-T network," *Proc. 11th Annual Conf. Information Fusion*, Cologne, Germany, 2008.

[9] Erdinc, O., Willett, P., and Bar-Shalom, Y.; "The Bin-Occupancy Filter and Its Connection to the PHD Filters," *IEEE Trans. Signal Processing*, Vol. 57, No. 11, pp. 4232- 4246, 2009.

[10] Gerard, O., Coraluppi, S., Carthel, C., and Grimmett, D.; "Benchmark Analysis of NURC Multistatic Tracking Capability," *Proc. 9th Annual Conf. Information Fusion*, Florence, Italy, 2006.

[11] Hanselmann, T. and Morelande, M.; "Multiple target tracking with asynchronous bearings-only-measurements," *Proc. 10th Annual Conf. Information Fusion*, Quebec, Canada, 2007.

[12] Haworth C.D., Saint-Pern Y., Clark D.E., Trucco E., Petillot Y.R.; "Detection and Tracking of Multiple Metallic Objects in Millimetre-Wave Images", *International Journal of Computer Vision*, Vol.71 No. 2, p.183-196, February 2007.

[13] Julier, S. and Uhlmann, J. "Unscented filtering and nonlinear estimation," in *Proc. IEEE*, vol. 92, no. 3, pp. 401–422, 2004.

[14] Lin L.; Bar-Shalom, Y.; Kirubarajan, T; "Track labeling and PHD filter for multitarget tracking," *IEEE Trans. Aerospace & Electronic Systems*, Volume 42, Issue 3, July 2006 Page(s):778 - 795.

[15] Kirubarajan, T., and Bar-Shalom, Y., "Tracking evasive move-stop-move targets with an MTI radar using a VS-IMM estimator," in *IEEE Trans. Aerospace & Electronic Systems*, vol. 39, no. 3, pp. 1098–1103, 2003.

[16] Mahler R.; "Multi-target Bayes filtering via first-order multi-target moments", *IEEE Trans. Aerospace & Electronic Systems*, Vol. 39, No. 4, pp. 1152-1178, 2003.

[17] Mahler, R.; "PHD filters of higher order in target number", *IEEE Transactions on Aerospace and Electronic Systems*, Volume 43, Issue 4, October 2007 Page(s):1523 - 1543.

[18] Mahler R.; *Statistical Multisource Multitarget Information Fusion*, Artech House, 2007

[19] Musicki D., Evans R., and Stankovic S., "Integrated probabilistic data association," I*EEE Trans. Automatic Control*, vol. AC-39, no. 6, pp. 1237–1241, 1994.

[20] Okello N., and Pulford G.; "Simultaneous registration and tracking for multiple radar with clutter measurement," *Proc. IEEE Signal Processing worshop on Statistical Signal and Array Processing*, Page(s) 60-63, 1996.

[21] Pannetier, B., Benameur, K., Nimier, V., and Rombaut, M., "VS-IMM using road map information for a ground target tracking," *Proc. 8th International Conference on Information Fusion*, 2005.

[22] Panta, K., Vo B.-N., and Singh S.; "Improved PHD filter for multi-target tracking," in *Proc. Intl. Conference on Intelligent Sensing and Information Processing*, Bangalore, India, pp. 213–218, 2005.

[23] Panta, K., Vo B.-N., and Singh S.; "Novel data association schemes for the Probability Hypothesis Density filter," *IEEE Trans. Aerospace & Electronic Systems*, Vol. 43, No. 2, pp. 556-570, 2007.

[24] Panta K., Clark D.E., and Vo B.-N.; "An Efficient Track Management Scheme for the Gaussian-Mixture Probability Hypothesis Density Tracker," *IEEE Trans. Aerospace & Electronic Systems*, 2008 (to appear).

[25] Pasha A., Vo B.-N., Tuan H.D., and Ma W.-K;, "Closed-form solution to the PHD recursion for jump Markov linear models," *Proc. 9th Annual Conf. Information Fusion*, Florence, Italy, 2006.

[26] Popp, R.L., Pattipati, K.R., and Bar-Shalom, Y.; "m-best S-D assignment algorithm with application to multitarget tracking," *IEEE Trans. Aerospace & Electronic Systems*, Vol. 37, No. 1, pp. 22- 39, 2001.

[27] Robert C., *The Bayesian Choice: a Decision-Theoretic Motivation*, First edition: Springer-Verlag, New York, 1994.

[28] Schuhmacher D., Vo B.-T., and Vo B.-N., "A consistent metric for performance evaluation of multi-object filters," *IEEE Trans. Signal Processing*, Vol. 56, No. 8 Part 1, pp. 3447- 3457, 2008.

[29] Sidenbladh H.; "Multi-target particle filtering for the Probability Hypothesis Density," in *Proc. Int'l Conf. on Information Fusion*, Cairns, Australia, pp. 800–806, 2003.

[30] Stoyan D.; Kendall D. and Mecke J.; *Stochastic Geometry and its Applications*, John Wiley & Sons, 1995.

[31] Tobias M. and Lanterman A.; "A Probability Hypothesis Density-based multitarget tracking with multiple bistatic range and doppler observations," in *Proc. IEE Radar Sonar and Navigation*, vol. 152, no. 3, pp. 195–205, 2005.

[32] Ulmke, M., and Koch W.; "On road-map assisted GMTI tracking," *1Proc. German Radar Symposium*, Page(s):614-621, 2004.

[33] Ulmke, M.; Erdinc O.; Willett, P.; "Gaussian mixture cardinalized PHD filter for ground moving target tracking," *10th International Conference on Information Fusion*, 9-12 July 2007 Page(s):1 - 8.

[34] Vo B.-N, Singh S., and Doucet A.; "Sequential Monte Carlo methods for multi-target filtering with random finite sets," in *IEEE Trans. Aerospace & Electronic Systems*, vol. 41, no. 4, pp. 1224–1245, 2005.

[35] Vo, B.-N.; Ma, W.-K.; "The Gaussian mixture Probability Hypothesis Density filter," *IEEE Trans. Signal Processing, IEEE Trans. Signal Processing*, Vol. 54, No. 11, pp. 4091-4104, 2006.

[36] Vo B.-T., Vo B.-N., and Cantoni A.; "Analytic implementations of the Cardinalized Probability Hypothesis Density Filter," *IEEE Trans. Signal Processing*, Vol. 55, No. 7, Part 2, pp. 3553-3567, 2007.

[37] Vo B.-T., Vo B.-N., and Cantoni A.; "Bayesian Filtering with Random Finite Set Observations," *IEEE Trans. Signal Processing*, Vol. 56, No. 4, pp. 1313-1326, 2008.

[38] Vo B.-T.; *Random Finite Sets in Multi-Object Filtering,* PhD Thesis, University of Western Australia, 2008.

[39] Zajic T., Ravichandran R., Mahler R., Mehra R., and Noviskey M.; "Joint tracking and identification with robustness against unmodeled targets," in *Signal Processing, Sensor Fusion and Target Recognition XII, SPIE Proc*., vol. 5096, pp. 279–290, 2003.

LIST OF FIGURES

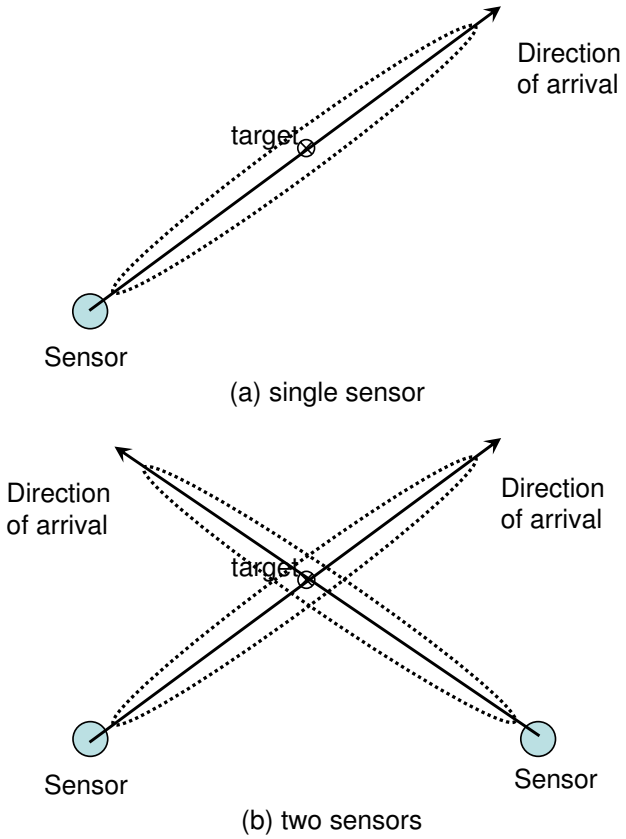

Fig. 1. Single and multiple sensors for direction of arrival measurements. Angular errors are approximated with Gaussian shapes.

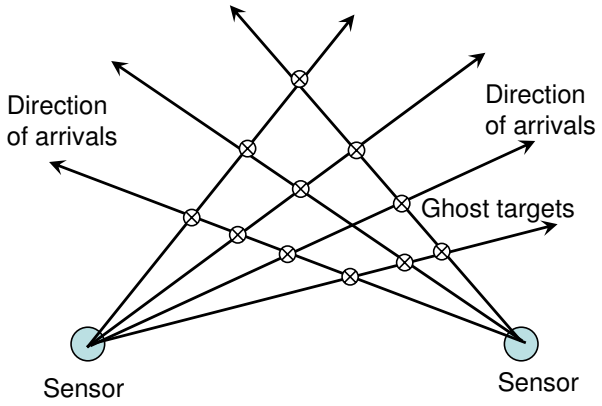

Fig. 2. Multiple sensor with cluttered direction of arrival measurements and ghost targets. Which is the true target?

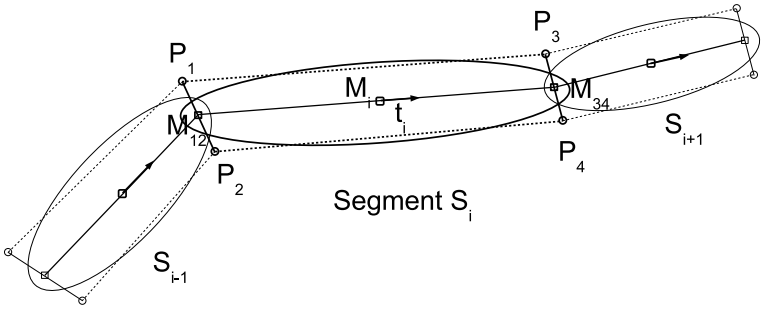

Fig. 3. Road model. Roads consist of trapezoidal segments with tangent through the midpoint M of trapezoidal input (P_1,P_2) and output points (P_3,P_4).

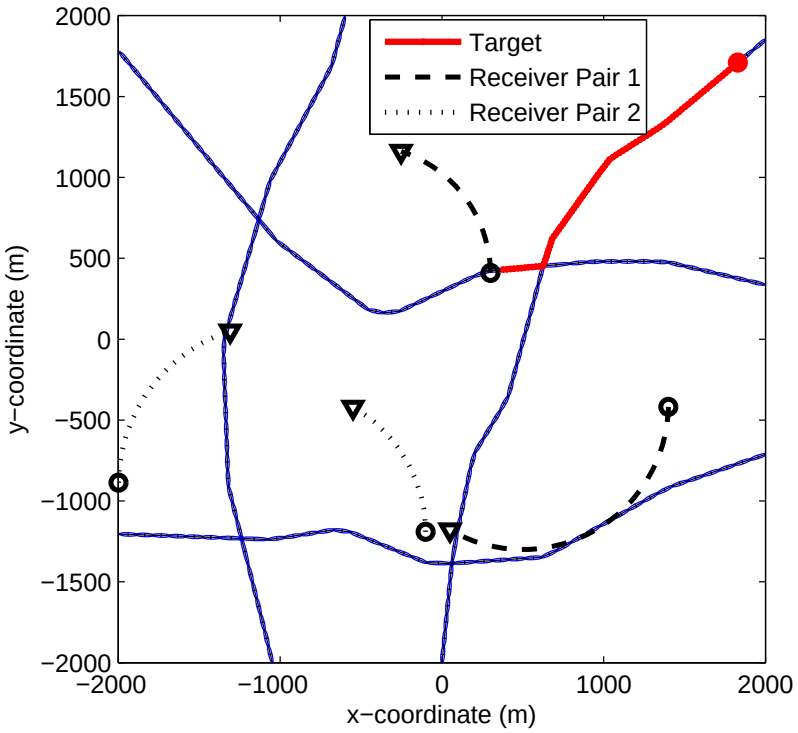

Fig. 4. Road network (blue) and target track (thick red line) and receiver trajectories (black dotted and dashed lines). The circles and triangles mark the starts and ends of the sensor trajectories.

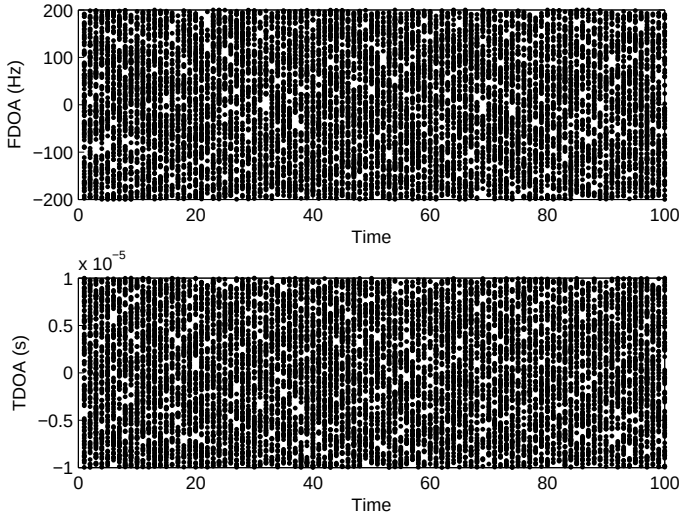

Fig. 5. FDOA/TDOA measurements versus time for receiver pair or virtual sensor 1

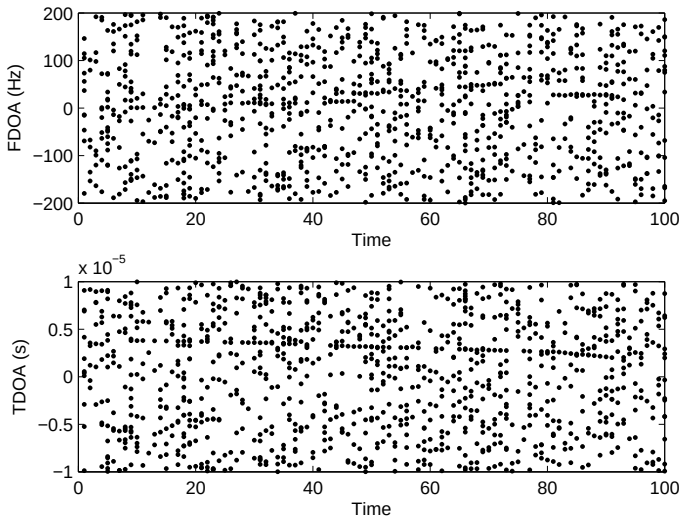

Fig. 6. FDOA/TDOA measurements versus time for receiver pair or virtual sensor 2

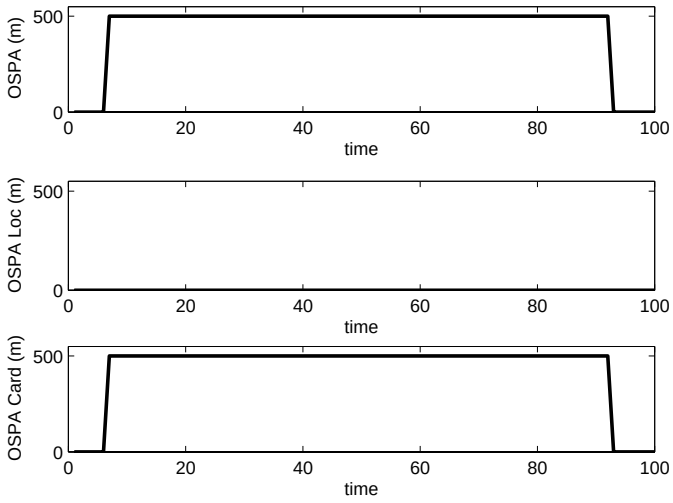

Fig. 7. OSPA error versus time for filtering, without road map information, using measurements from virtual sensors 1 and 2.

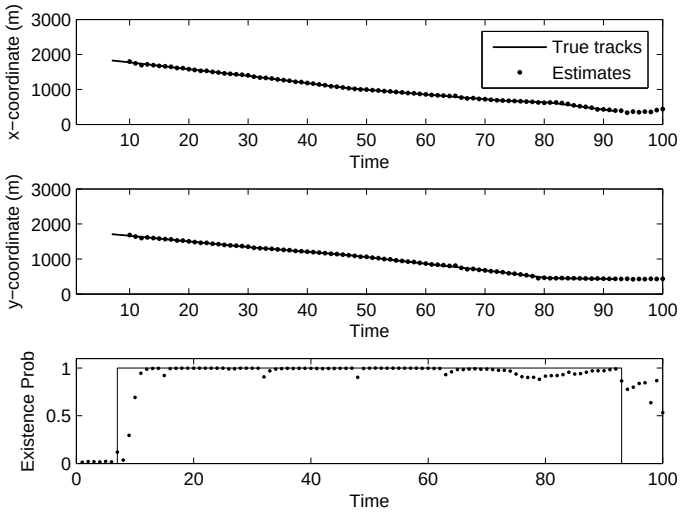

Fig. 8. Filter output versus time, with road map information, using measurements from virtual sensor 1.

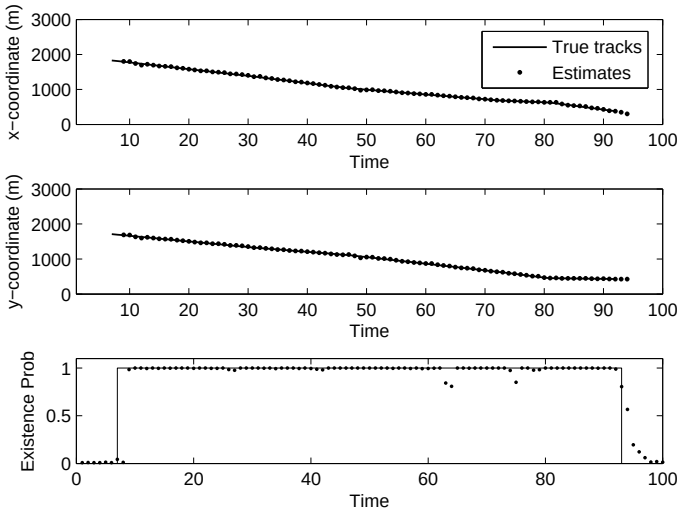

Fig. 9. Filter output versus time, with road map information, using measurements from virtual sensors 1 and 2.

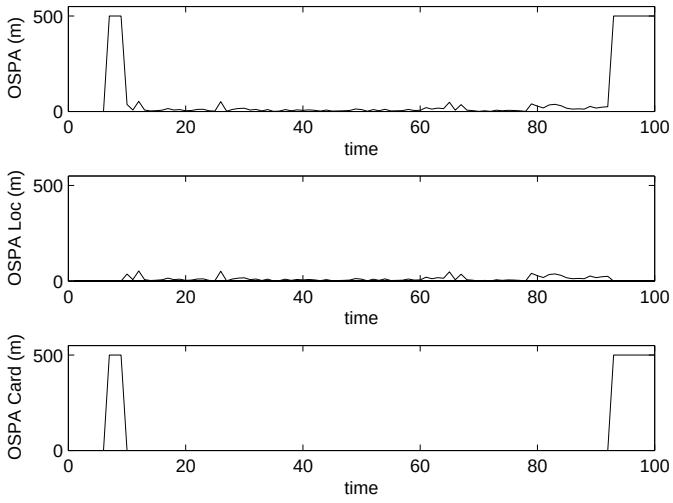

Fig. 10. OSPA error versus time for filtering, with road map information, using measurements from virtual sensor 1.

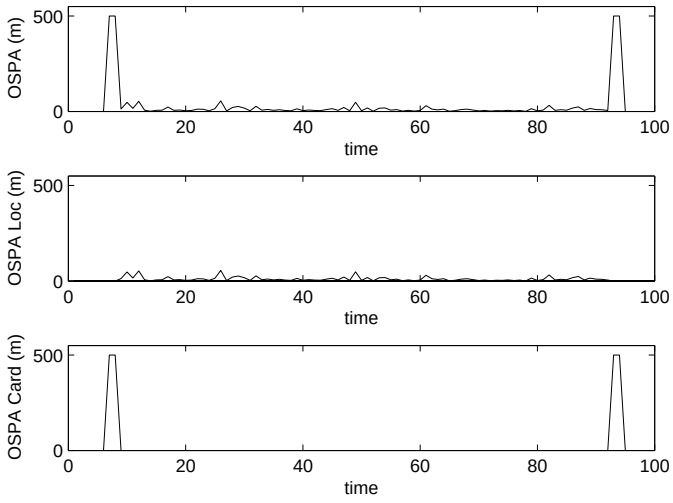

Fig. 11. OSPA error versus time for filtering, with road map information, using measurements from virtual sensors 1 and 2.

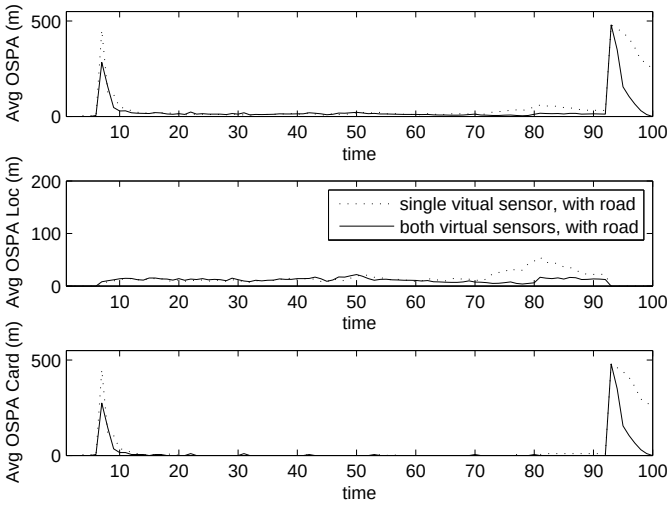

Fig. 12. Mean OSPA error versus time for filtering with a single virtual sensor and both virtual sensors.

Ba-Tuong Vo was born in Perth, Australia, in 1982. He received the B.Sc. degree in applied mathematics and B.E. degree in electrical and electronic engineering (with first-class honors) in 2004 and the Ph.D. degree in engineering (with Distinction) in 2008, all from the University of Western Australia, Crawley. He is currently an Assistant Professor and Australian Postdoctoral Fellow in the School of Electrical, Electronic and Computer Engineering at the University of Western Australia. His primary research interests are in point process theory, filtering and estimation, and multiple object filtering. Dr. Vo is a recipient of the 2010 Australian Museum Eureka Prize for Outstanding Science in Support of Defence or National Security.

Chong Meng Samson See (M'92) was born in Singapore on June 13, 1968. He received the Diploma degree in electronics and communications engineering (with merit) from Singapore Polytechnic in 1988 and the M.Sc. degree in digital communication systems and the Ph.D. degree in electrical engineering, both from the Loughborough University of Technology, Loughborough, U.K., in 1991 and 1999, respectively. Since 1992, he has been with DSO National Laboratories, Singapore, where he is now a Distinguished Member of Technical Staff and is currently leading a team in the research and development of advanced array signal processing systems and algorithms. He also holds an adjunct appointment at Temasek Laboratories, Nanyang Technological University, as a Principal Research Scientist, where he leads a program on sensor array research. His research interests include the area of statistical and array signal processing, communications, and bio-inspired systems. He has two issued patents on direction finding. Dr. See is an Associate Editor of the IEEE TRANSACTIONS ON SIGNAL PROCESSING and a member of the IEEE Sensor Array and Multichannel Signal Processing Technical Committee.

Ma Ning received her BEng and MEng from Northwestern Polytechnical University, China in 1983 and 1986 respectively, and PhD from Institut Nationale des Sciences Appliquees de Lyon, France, in 1996. She worked as a lecturer in Northwestern Polytechnical University from 1986 to 1992. She was a research associate in Chinese University of Hong Kong, in 1997. From 1998, she has been working in DSO National Laboratories and is a Principal Member of technical Staff. She is a Senior Member of IEEE. Her research interest includes array signal processing and its application in sonar, and sonar image processing.

Wee Teck Ng graduated with a Ph.D. from Nanyang Technological University, Singapore in 2005. His main research interests are in communication theory. He was with the Centre for Strategic Infocomm Technologies from 2004 to 2007. He is currently working at DSO National Laboratories Singapore and is concurrently an adjunct staff with Temasek Laboratories at Nanyang Technological University.